Journal of Inorganic and Organometallic Polymers and Materials (2020) 30:3574–3585
https://doi.org/10.1007/s10904-020-01513-w

Polysiloxane Derived Macroporous Silicon Oxycarbide Microspheroidal Particles and Their Decoration with 1D Structures

W. Fortuniak[1] · J. Chojnowski[1] · U. Mizerska[1] · P. Pospiech[1,2] · J. Zakrzewska[1] · S. Slomkowski[1]

Received: 24 January 2020 / Accepted: 19 March 2020 / Published online: 28 March 2020

Abstract
A simple method of synthesis for the macroporous SiOC spheroidal microparticles was developed. Preceramic polysiloxane macroporous microbeads were obtained by a one-step aqueous emulsion process involving poly(hydromethylsiloxane) (PHMS) with the addition of $FeCl_3 \cdot 6H_2O$. Thermal treatment of these particles gave various SiOC materials depending on the pyrolysis temperature. Hierarchically porous spheroidal mezo-macroporous ceramers were obtained at 600 °C. Heating at 850–1000 °C gave SiOC ceramic spheroidal particles with about 60% open porosity. Ceramization at 1200–1400 °C led to the particles decorated with ceramic whiskers and wires. Heating at 1600 °C gave wires and spilled ceramic particles. These 1D ceramic structures were formed by a Vapor–Liquid–Solid (VLS) mechanism.

Keywords Ceramic macroporous beads · VLS growth structures · Macroporous SiOC particles · Porous ceramers · Polymer derived macroporous SiOC

1 Introduction

Polymer-derived SiOC ceramics are a fast developing field of materials science with great perspectives for application in many areas of advanced technologies [1]. Among various structures of these materials, ceramic beads of micrometric sizes having opened macropores are very promising for many practical uses. SiOC ceramics have excellent chemical and thermal stability, high mechanical strength and very good biocompatibility. Open macropores ensure easy transport and create large areas of the particle surface and facile contact with them. Macroporous beads prepared of various ceramic materials have potential as catalysts [2, 3], enzyme supports [4], microorganism carriers [5], refractory materials [6], absorbers and materials for chromatography [7, 8], sensors [9], materials for tissue engineering [10] and for other biomedical applications [11]. Preparation of polymer-derived macroporous silicon oxycarbide particles of regular spheroidal shapes are a challenge and require special synthetic methods. They can be fabricated by ceramization of macroporous silicone resin microspheres obtained by a two-step formation of a double emulsion water-in-oil-in-water system. After heating at 1200 °C particles of ~ 200 µm in size preserved their close to spherical shape and had a total porosity of ~ 80 vol% [12]. Regular macroporous spherical particles were obtained when the double emulsion method was combined with a microfluidic technique. After heating at 1000 °C, they were 55–110 µm in diameter, showed a very small size dispersion and open macropores of 1–10 µm [13]. Ceramic microspheres with control porosity were obtained by emulsion-ice templating [14]. A combination of a carbosilane polymer emulsion processing and freeze-drying was used for the preparation of 1–2 mm macroporous beads. Their thermal treatment gave hierarchically macro-mezo-microporous spheroidal ceramic particles [15]. Spheroidal particles were obtained from a methylsilsesquioxane resin using an electrohydrodynamic method. The ceramic SiOC particles formed had a mean size of 3 mm and spherical large cells interconnected by 1.3 µm channels to form an open pore system [16]. We have recently described a method for the generation of macroporous microspheroidal particles by a simple one-pot emulsion processing of linear siloxane polymer [17]. The addition of inorganic salts to the

✉ J. Chojnowski
jchojnow@cbmm.lodz.pl

[1] Center of Molecular and Macromolecular Studies, Polish Academy of Sciences, 112 Sienkiewicza, 90-363 Lodz, Poland

[2] Present Address: Centre of Papermaking and Printing at Lodz University of Technology, 223 Wólczanska, 90-924 Lodz, Poland

polysiloxane polymer before emulsification in aqueous system led to a double emulsion in which the polymer spherical microparticles contained dispersed nanodroplets of the salt aqueous solution. The osmotic pressure led further to the formation of open or partly open macropores in the formed polymer microspheroidal particles. In this paper we report the ceramization of these beads to fabricate SiOC ceramic particles of nearly spherical shape having open macropores. Under certain conditions of ceramization, the presence of dispersed metal salt in these particles led to their decoration with the formation of nano-whiskers or wires. It is noteworthy that there has recently been interest in ceramics enriched in D1 structures because of their electromagnetic wave absorption properties [18–20] and high catalytic efficiency [21].

2 Experimental Procedures

2.1 Materials

Polyhydromethylsiloxane, PHMS, terminated by trimethylsiloxane groups, with a molecular mass of ~ 2000 was purchased in ABCR (HMS 991), and 1,3-divinyltetramethyldisiloxane, DVTMDS, was product of ABCR with a declared purity of 97%. Poly(vinylalcohol) (purity 99.5%) was obtained from POCH Gliwice. Platinum Karstedt complex solution containing 20 w% of Pt was kindly offered by Momentive Leverkusen. $FeCl_3 \cdot 6H_2O$ was obtained from Sigma Aldrich (ACS reagent, 97%). 1,4-Dioxane (p.a.) has a declared purity of 99.8%.

2.2 Physical Methods

^{29}Si MAS NMR spectra of preceramic particles were obtained with a DSX 400 Bruker spectrometer working at 59.627 MHz in CP (cross-polarization) mode. The content of reactive groups, SiH and SiOH and cross-links in the microspheres, were calculated from the integration of the respective peaks with correction for peak integration using HPDec (single pulse excitation) spectrum, as previously described [22, 23]. SEM images were recorded using a Jeol JSH 5500 LV microscope in high vacuum mode at the accelerated voltage of 10 kV. Samples were coated with a fine layer of gold (about 20 µm thick), using the ion coating JEOL JFC 1200 apparatus. SEM–EDS spectra were recorded with the JEOL ISM-6010LA (JEOL, Japan) scanning electron microscope equipped with an energy-dispersive X-ray detector. Prior to examination, sample surfaces were vacuum sputtered with a 5 nm gold layer (Quorum EMS150R ES, UK). Thermal analysis of polysiloxane microspheres was carried out on a TGA 2950 Hi-Res analyzer (TA Instruments, USA) using 20 mg samples heated in a nitrogen atmosphere. XRD pattern was obtained with a PANalytical X'Pert Pro MD diffractometer with a Cu K_{al} X-ray line using step size 0.016° and 30 s step time.

2.3 Dilatometry Measurements of Porosity

Total porosity of powder, P_{tot}%, was calculated according to Eq. 1 and open porosity of particles, P_{open}%, by Eq. 4.

$$P_{total}\% = 100 \times \left(1 - \rho_{bulk}/\rho_{true}\right) \quad (1)$$

$$\rho_{bulk} = \delta \times \rho_{powder} \quad (2)$$

$$\delta = \left(\rho_{true}/\rho_{powder}\right)_{non-porous} \quad (3)$$

$$P_{open}\% = 100 \times \left(1 - \rho_{bulk}/\rho_{skeletal}\right) \times 100 \quad (4)$$

where ρ_{powder} is apparent powder density, ρ_{bulk} is bulk density of particles including their solid skeletons and opened and closed pores while δ is coefficient allowing for free space between particles in the powder. The ρ_{true} is the bulk density of corresponding non-porous particles. The $\rho_{skeletal}$ is the apparent skeletal density of particles without open pores, but including closed pores.

To determine the apparent powder density, $\rho_{powder,}$ a glass cylinder of 4 mm diameter was filled with a known weight of ceramic powder and subjected to shaking and vibration keeping the cylinder in perpendicular position until the level of the powder was not changed. The height of the powder column in the cylinder was measured and its volume was calculated. Hence the apparent powder density was found. To calculate ρ_{bulk}, the σ coefficient was estimated to be 1.608 by comparison of apparent powder density with the true densities of the non-porous polysiloxane microspheres that were heated for 1 h at 1000 °C in the argon atmosphere. It was assumed that the particles heated under these conditions were not porous [24]. The skeletal density of the ceramic particles was determined at 25 °C using a 3 mL dilatometer, which was weighed empty, then filled with n-heptane and then filled with the suspension of known weight of the measured ceramic porous particles in this solvent. The suspension was kept in the dilatometer for at least 24 h occasionally connecting it to vacuum to remove air bubbles from the material pores. The apparent skeletal density, $\rho_{skeletal}$, was calculated using Eq. 5. This was the density of the material forming the skeleton of the particle, which also contained closed pores. It also contained the fraction of the open pores, which were not accessible for n-heptane. Due to the viscosity and surface tension of this solvent, very small micropores or those pores connected by very narrow channels might remain unfilled.

$$\rho_{skeletal} = M_p \times \rho_s / M_s + M_p - M_{p+s} \quad (5)$$

where M_p, M_s and M_{p+s} are weights in dilatometer of porous particles, solvent and particles suspension in the solvent respectively, and ρ_s is the solvent density. The density of non-porous particles was measured by dilatometry in an analogous way. Some of the data were taken from Ref. [25].

2.4 Mercury Intrusion Measurements of Porosity

Mercury intrusion porosity data were collected with a Micrometrics Instrument AutoPore IV 9500 V 1.07 operating at the pressure of 0.001 to 100 MPa and measuring pores of diameters above 3.5 nm. Pore intrusion was determined as the difference between total intrusion at maximum pressure (100 MPa) and the intrusion into the space between particles (0.2 MPa). The open pore porosity was calculated from the pore intrusion. Samples A2 and A3 were analyzed with a Micromeritics Autopore IV 9520.

2.5 Ceramization

The pyrolytic processes were performed in Nabertherm RHTH 120/300/18 furnace according to the procedure described in Ref. [23]. A weighed sample was placed in aluminum oxide vessel (DEGUSSIT® AL23) and heated in a flow of argon (100 L/h). The temperature was increased at the rate of 5 °C/min and a target temperature was kept for 1 h or for 5 h. The furnace was allowed to cool to the room temperature with a continuous argon flow. The material that was obtained was weighed and characterized.

2.6 Preparation of Preceramic Materials

Porous polysiloxane microspheroidal particles were prepared by a method similar to that described earlier [17]. Typically, a solution of PHMS (24 g), DVTMDS (5.4 g), Karstedt complex containing 4.2×10^{-4} g Pt in 20 mL of dioxane was stirred at 45 °C. After 14 min. a solution of $FeCl_3 \cdot 6H_2O$ (1.6 g in 12 mL of dioxane) was added and after 1 min. the solution formed was homogenized at 45 °C for 120 s at 8000 rpm with 400 mL of deionized water containing dissolved PAV (1.6 g). The formed emulsion was diluted with 1200 mL of deionized water containing PAV (4.8 g) and stirred gently at 45 °C for 120 h. Particles were separated and subjected to several cycles of washing with water and centrifuging. The particles were then subjected to liofilization to yield the macroporous spheroidal particles (25.5 g) which were further analyzed and used in ceramization. Two samples were prepared with the $FeCl_3 \cdot 6H_2O$ addition; a separate sample was prepared without salt addition, Table 1.

Table 1 Synthesis of precursor

Sample	PHMS g	DVTMDS g	$FeCl_3 \cdot H_2O$ g	Pt mol	Dioxane g
A	24	5.4	1.60	2.2×10^{-6}	32
B	24	5.4	0.40	3.0×10^{-6}	32
C	48	11.0	0	4.6×10^{-6}	40

3 Results and Discussions

3.1 Formation of Polysiloxane Almost-Spherical Macroporous Particles—Ceramic Precursors

Polysiloxane preceramic macroporous microspheroidal particles were obtained by emulsion processing of polyhydromethylsiloxane crosslinked in situ by hydrosilylation of 1,3-divinyltetramethyldisiloxane catalyzed by a Pt(0) complex. It was reported elsewhere [17, 26] that the addition of various salts, such as $NiCl_2 \cdot 6H_2O$, $FeCl_3 \cdot 6H_2O$, $PdCl_2$ and $AgNO_3$, to the solution of the precursor polymer allows to obtain macroporous polysiloxane microspheres. The iron chloride hydrate was used in this research because it is well miscible with the polymer dioxane solution. Macropores were generated by the addition of $FeCl_3 \cdot 6H_2O$ to the solution of precursor polysiloxane polymer [17]. During mechanical emulsification of this solution in water, nanodroplets of the concentrated salt solution dispersed in polysiloxane microspheres were formed. Hydrolysis of SiH groups in the polymer proceeded in parallel to its crosslinking thereby producing a number of hydrophilic SiOH groups on the polymer, thus giving the possibility of migration of outside water to the salt solution nanodroplets due to osmotic pressure. The microspheres are swelling, which leads further to their deformation and the generation of open pores. The increase in volume of the droplets is accompanied by polymer crosslinking, which provokes a strain on the spheroidal particles. Channels are formed between the nanodroplets through which the salt solution migrates out of the swollen particle under the pressure built up by an increase in droplet volume. Spheroidal, large pores are generated, which are interconnected by channels to form an open pore system. The macroporous preceramic spheroidal particles are displayed in Fig. 1a and b.

^{29}Si NMR studies show that the precursor polysiloxane microspheroidal particles retain a large number of SiH and SiOH reactive groups. The contents of these groups calculated from ^{29}Si NMR spectra are summarized in Table 2. Since condensation processes of these reactive groups and silylation reaction occur during the precursor formation, the siloxane polymer in these precursor beads is strongly crosslinked by both SiOSi and $[(CH_2CH_2)(CH_3)_2Si]_2O$ bridges (Table 1). Moreover, the reactivity of water in

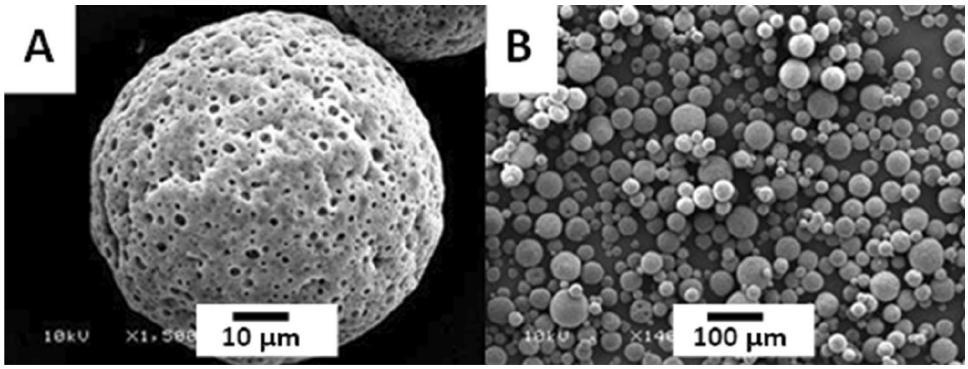

Fig. 1 **a**, **b** Micrographs of preceramic microspheres generated by emulsion process from PHMS and DVTMDS as crosslinker with the addition of $FeCl_3 \cdot 6H_2O$

Table 2 Comparison of chemical structure of polysiloxane microspheres synthesized: A—with the addition of $FeCl_3 \cdot 6H_2O$ and C—without addition of the salt

Sample	Functional groups		Cross-links	
	SiH %	SiOH %	SiOSi %×2	SiCCSi-OSiC-CSi %×2
A	52.9	18.7	17.4	11.0
C	8.9	53.4	21.7	16.0

nanodroplets are decreased by the salt and the conversion of SiH groups to SiOH is lower than in microspheres prepared without using the salt.

3.2 Preparation and Studies of Ceramic Particles

The presence of the iron salt in the polysiloxane microspheres has an impact on their pyrolytic processes, which is demonstrated by comparison of the thermogravimetric curves of these materials with the microspheres not containing the iron salt, Fig. 2. Thus, the weight decreases in the range 150–250 °C more rapidly for the latter because they contain a larger number of SiOH groups and consequently more water. However, on further heating to 600 °C, the decomposition of the polymer is faster and deeper in the presence of $FeCl_3 \cdot H_2O$. Evidently the salt and/or its metabolites promote the material decomposition.

The preceramic macroporous spheroidal particles were pyrolyzed at 600, 850, 1000 and 1200 °C under argon. The morphology of the pyrolyzed samples was studied by SEM, mercury porosimetry and dilatometry. Representative SEM micrograms are shown in Fig. 3a–h. The distribution of sizes of some of these materials are displayed in Fig. 4 a and b.

Microspheroidal shapes of particles are well-retained on heating at 600 °C and on the ceramization processes at 850–1200 °C. The particles also preserve their macroporous structure. As seen in Fig. 3d, the large, almost spherically shaped pores are connected by channels. The pore system

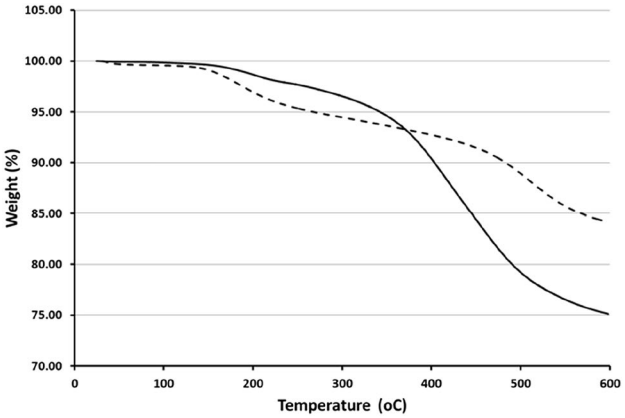

Fig. 2 Comparison of thermogravimetric plots for microspheroidal particles obtained with the addition of $FeCl_3 \bullet 6H_2O$ (solid line) with the microspheres generated without the iron salt (dashed line). The rate was 5 °C/min

is mostly opened, which is confirmed by dilatometry measurements (Table 3) and by mercury porosimetry studies (Table 4).

There is fairly good agreement between the open porosity determined by both methods. The open porosity is close to the total porosity measured by dilatometry, which means that the contribution from the closed pores to the total porosity is low. The macroporosity in the pyrolyzed microspheres is high at all the temperatures studied. The decrease is seen in the sample heated at 1200 °C. The average pore diameter of samples heated at 850–1000 °C is ~ 0.25 µm and increases for the sample heated at 1200 °C (Table 4).

The material heated at 600 °C is distinguished by a large area of pores, 178 m^2/g, and a much smaller average diameter as compared to those pyrolyzed at a higher temperature, although the pore volume remains at the same level. These results suggest that, besides macropores responsible for the large open pore volume, there are mezo-pores of sizes greater than 3.5 nm. In addition, the adsorption of N_2 gas was performed and gave an area of 477 m^2/g as calculated by the BET method (Langmuir method gave 643 m^2/g).

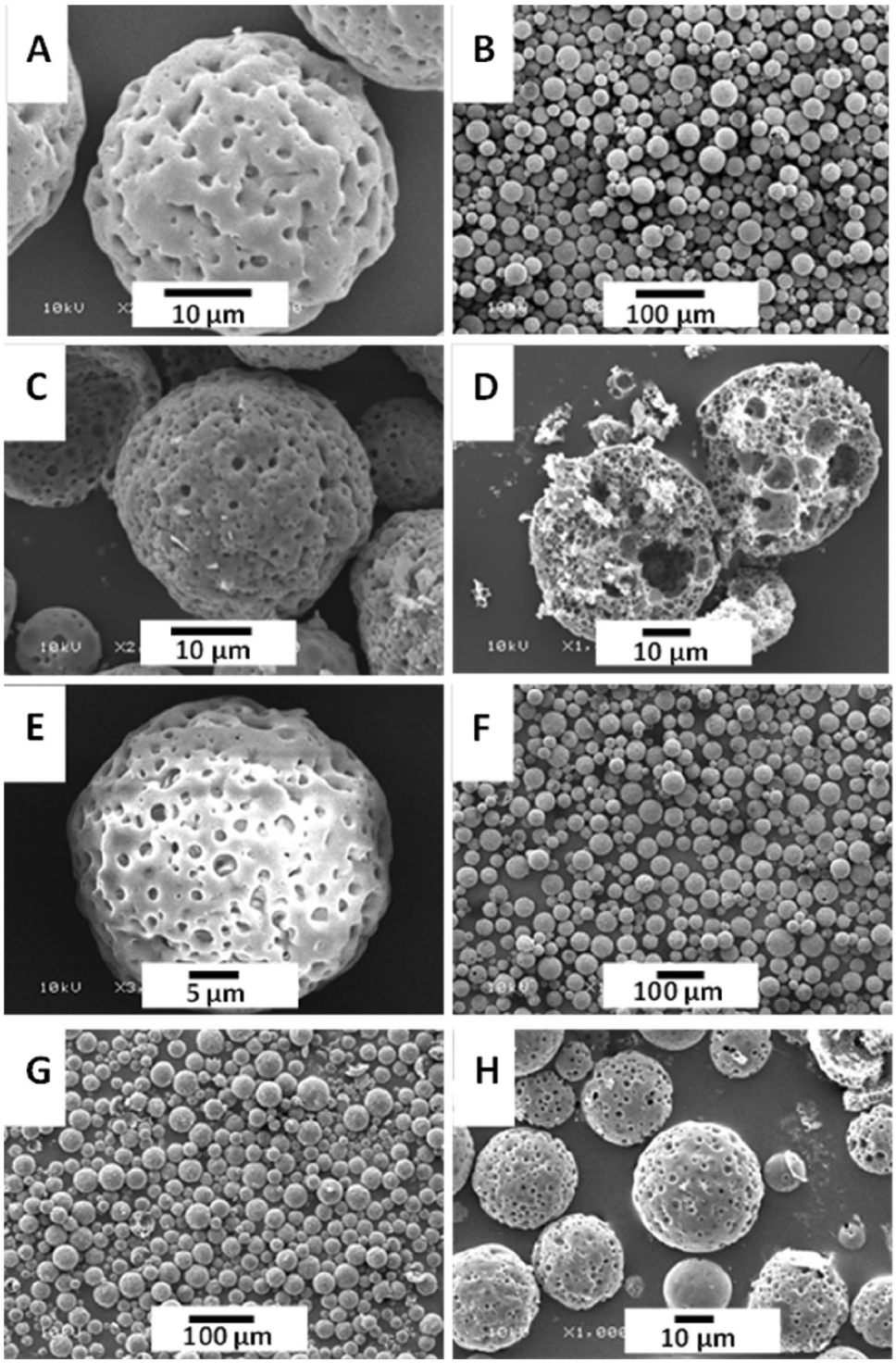

Fig. 3 **a**–**h** Micrographs of the spheroidal particles generated from PHMS/DVTMDS with $FeCl_3 \cdot 6H_2O$ heated in argon for 1 h at: **a** and **b** 600 °C, **c** and **d** 850 °C, **e** and **f** 1000 °C, **g** and **h** 1200 °C

The BET result, in comparison with the mercury intrusion data, corresponds to an area of 299 m^2/g of micro- and mezo-pores of sizes below 3.5 nm. It is well-known that polysiloxanes lose a portion of their organic moieties during heating at 600 °C and that the organic gases evolved at this temperature generate micro- and mezo-pores [24, 27, 28]. These pores disappear if the material is pyrolyzed at higher temperatures [24]. Since the instrument measures the intrusion of pores of diameters larger than 3.5 nm, smaller pores are not intruded. These are mostly mezo-pores, which are responsible for the large specific area of this material registered by the mercury porosimetry. Since macropores are well-retained in these particles, they exhibit hierarchical macro-mezo-microporosity. This hierarchical pore size

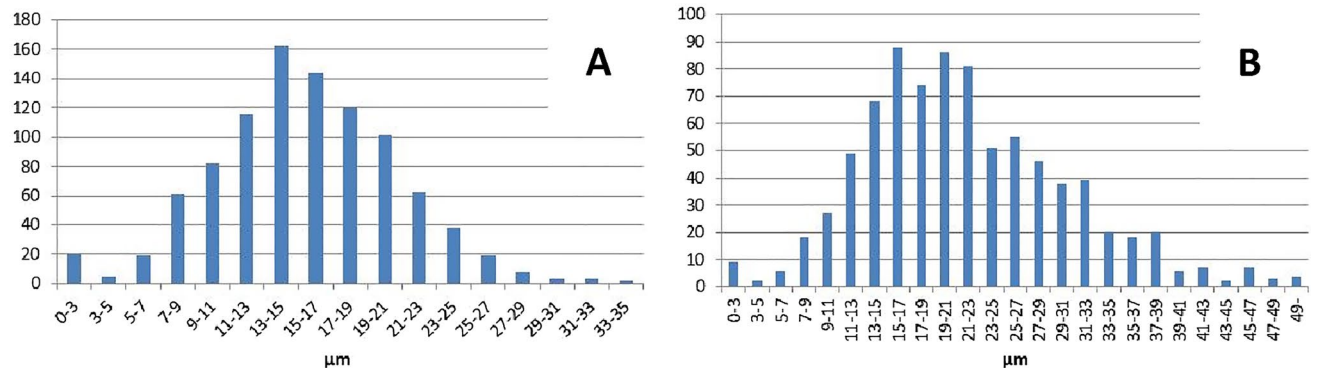

Fig. 4 **a**, **b** Size distribution of particles obtained by pyrolysis in argon for 5 h of polysiloxane microspheroidal particles at temperatures: **a** 600 °C, **b** 1000 °C

Table 3 Porosity and size of macroporous SiOC ceramic particles measured by dilatometry

Sample number	Ceramization temperature °C	Powder density ρ_{powder}	Bulk densit unporous ρ_{bulk}	Skeletal density $\rho_{skeleton}$	Open porosity Popen %	Total porosity P_{tot} %
A1	600	0.229	1.95[a]	1.38	73	81
A2	850	0.293	1.99	1.77	73	77
A3	1000	0.428	2.19[b]	1.92	64	69
A4	1200	0.552	2.26[b]	1.83	52	61
B1	850	0.456	1.99	n. d	n. d	63
B2	1000	0.483	2.19[b]	1.93	60	65

[a]Estimated from mass loss

[b]Values taken from Ref. [25]

Table 4 Mercury intrusion porosimetry data

Sample	Temperature of ceramization °C	Pore intrusion volume[a] mL/g	Total pore area[a] m^2/g	Opened porosity P_{opened}%	Average pore diameter (4 V/A) nm
A1	600	0.79	178 477[b]	61	49.1
A2	850	0.55	16.5	68	616
A3	1000	0.50	24.4	64	261
A4	1200	0.45	16.6	51	384
B1	850	0.84	34.8	63	266
B2	1000	0.79	29.7	63	259

[a]Measured in the pressure range of 0.2–100 mPa

[b]Measured by nitrogen gas adsorption and calculated by BET method

structure is well seen in Fig. 5a where a plot of cumulative pore area versus pore size diameter resulting from mercury intrusion studies is displayed. Additional nitrogen adsorption studies confirm the significant mezoporosity of the samples.

Particles heated at higher temperatures, i.e., 850–1200 °C [24], lose most of their micro- and mezoporosity, but retain macroporosity. Their intrusion volume is still high, but the pore area is much lower and the average pore diameter is larger (Table 3). This is also seen by a comparison of the cumulative pore area plots (Fig. 5a (600 °C), b (1200 °C)).

A considerable portion of the iron salt remains in beads after the emulsion process. This salt is subjected to reduction during pyrolysis, which may eventually lead to the formation of metal iron nanoparticles. Their interaction with the matrix produces iron silicides known to be catalysts for the generation of one-dimensional ceramic nanostructures

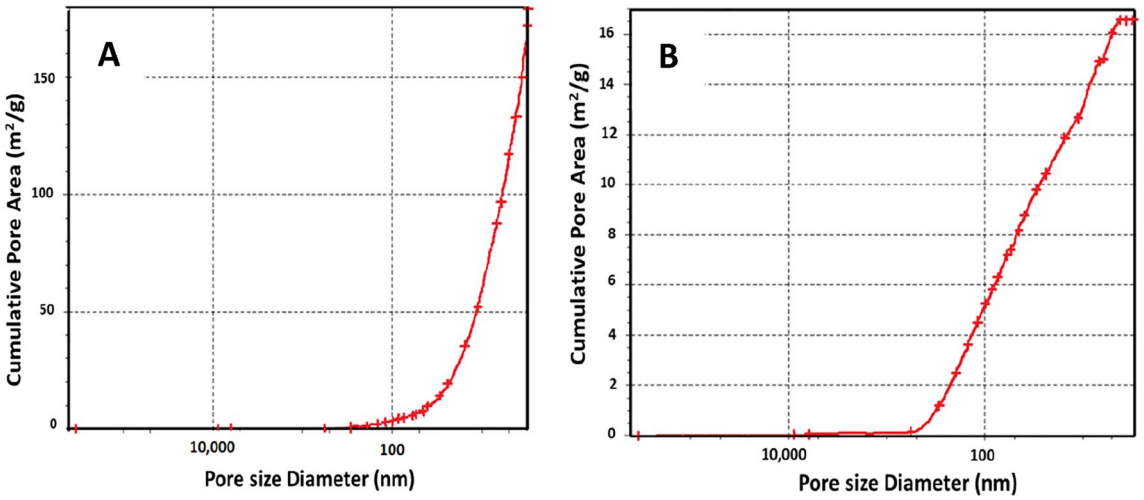

Fig. 5 **a**, **b** Cumulative pore area vs pore size for sample heated at: **a** 600 °C, **b** 1200 °C

[29, 30]. Since the SiFe binary system shows a eutectic point close to 1200 °C [30], this temperature could be the treshold point for the formation of these structures. Clear one-dimensional structures on the SiOC particles were not observed when the polysiloxane was ceramized in argon at 1200 °C for 1 h. However, the decrease in the volume of pores (Table 4) might come from the 1D structure formed inside the pores. Mushroom-type efflorescence was observed on surfaces of the ceramic particles after heating under the same conditions (argon 1200 °C) for 5 h (Fig. 6a, b). These structures grew from the external wall of the particles, had lengths up to a hundred nanometers and resulted with spheroidal heads (tips). Some particles that had smaller sizes were decorated with nanowhiskers with lengths of several micrometers (Fig. 6c, d).

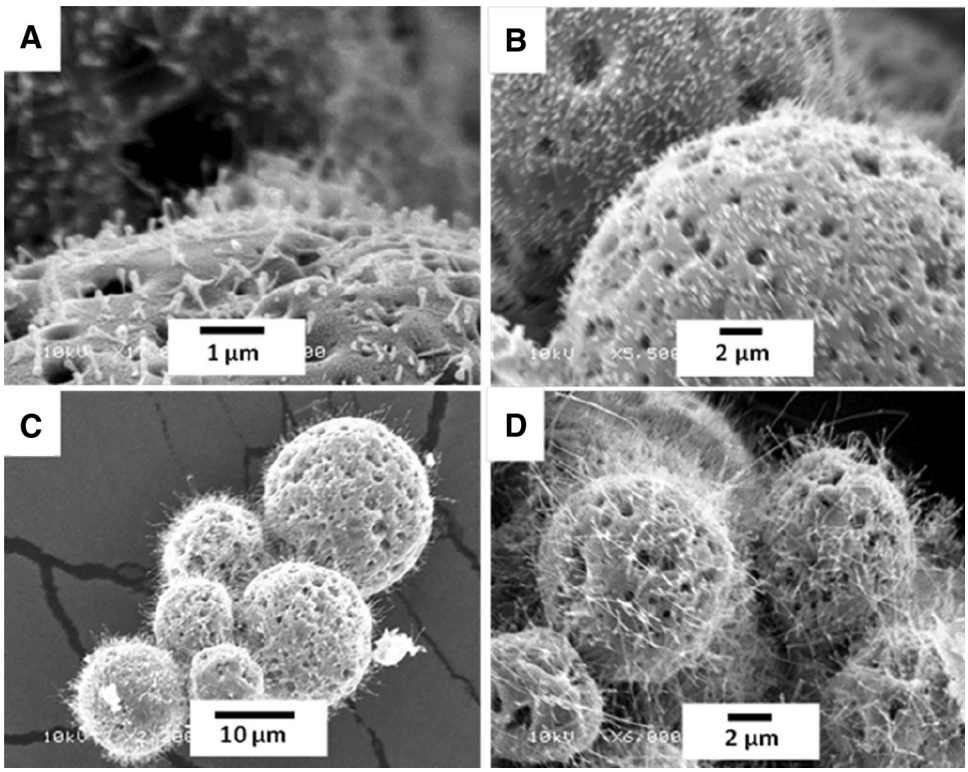

Fig. 6 **a**–**d** SEM micrograms of microspheres heated in argon at 1200 °C for 5 h

Polysiloxane microspheres containing the $FeCl_3 \cdot 6H_2O$ salt were also ceramized in argon for 5 h at 1400 °C and at 1600 °C respectively. Those heated at 1400 °C retained their spherical shape and 33.7% of their initial weight. SEM photograms of these particles reveal that some are decorated with wires which are up to micrometer thick and dozens micrometers long. They are terminated with tips, and most of them get out of pores (Figs. 7a, b).

The same polysiloxane microspheres lost over 95% of their initial weight during heating at 1600 °C for 5 h. Most of the ceramic particles were disrupted (Fig. 8c). On the other hand, a cobweb layer was deposited on the wall of the pipe of the furnace. SEM images of a sample of this material taken off the pipe wall are displayed on Fig. 8a and b. They show that the cobweb consists of nano- and micro-wires. They are mostly straight wires terminated with spheroidal tips, have thickness to 3 µm and some have lengths above 300 µm.

images the electron beam was focused on the same area including fragments of wires and their tips. Each of micrographs was taken with tuning of the electron beam energy to the signal of a studied element in the EDS spectrum shown in Figs. 9c and 10g. This allowed for mapping of the elements to find the elemental composition of the wires and their tips. A strong SiOC background made it difficult to map the wires on particles ceramized at 1400 °C. Regardless, the micrograms of a damaged sphere displayed in Fig. 9a and b showed that iron appears mostly on the wire tips. Small dots of iron are also scatter over the particle surface that might give rise to the formation of thin whiskers at 1200 °C, as seen in Fig. 6a–d.

Identification of various chemical elements using elemental mapping was also made for wires deposited on the furnace wall. Iron was observed only in the tips, while silicon appeared throughout wires including the tips. Other elements such as oxygen, carbon and aluminum were observed

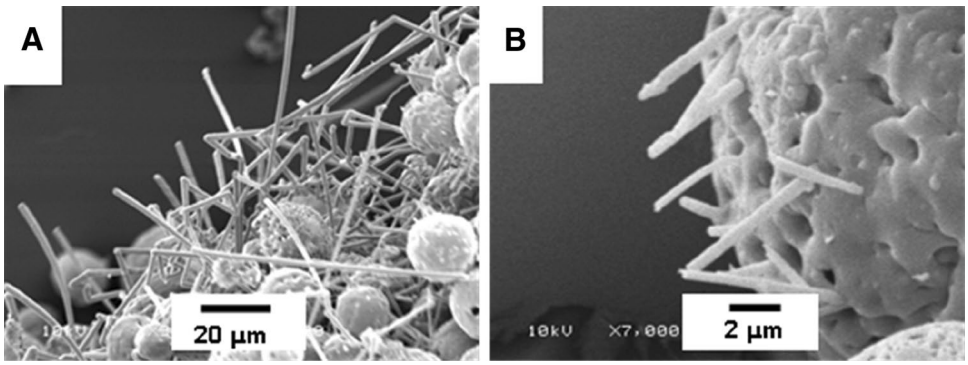

Fig. 7 **a**, **b** SEM micrograms of SiOC microspheres generated from polysiloxane microspheres ceramized at 1400 °C for 5 h in the atmosphere of argon

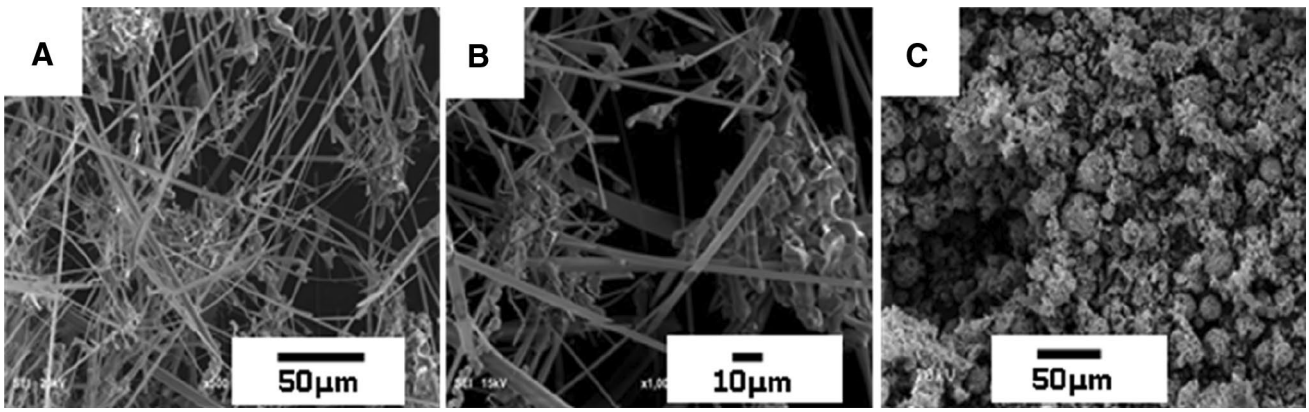

Fig. 8 **a**–**c** SEM micrographs of materials heated at 1600 °C in argon for 5 h, **a** and **b** micrographs of cobweb taken from the wall of furnace, **c** residual particles

The chemical structure of these wires was studied by energy dispersive x-ray spectroscopy, EDS. The results are displayed in Figs. 9a–c and 10a–g. In the recorded SEM

in the wires, but were absent in the tips. Thus, the tips consist of iron and silicon. The carbothermal reduction of silica takes place at temperatures 1200–1600 °C producing SiO

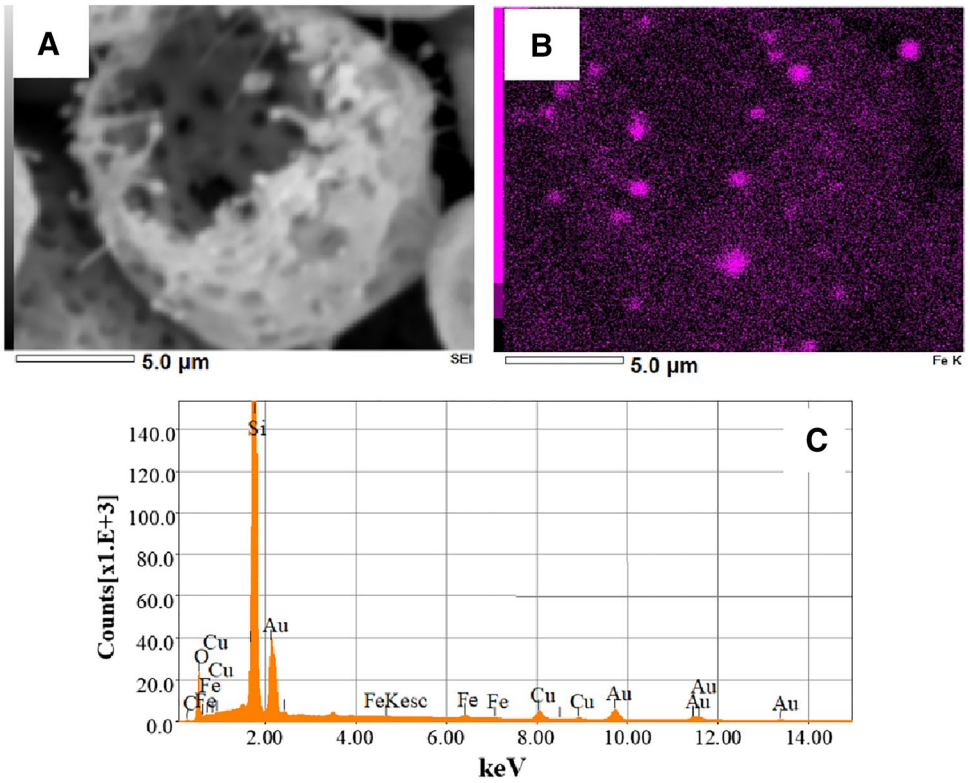

Fig. 9 **a–c** B mapping analysis of iron in damaged microsphere shown in SEM micrograph A, C is EDS spectrum of the sample fragment

and CO gaseous products and silicon carbide amorphous and crystalline phases [29, 31–33]. X-ray diffraction pattern of particles heated at 1400 °C is displayed in Fig. 11. The gaseous products are deposited on the iron-silicon droplets, which catalyze the formation of SiOC 1D structures. An interesting feature is the presence of aluminum in the formed wires at 1600 °C. The partial pressure of aluminum oxide, which originates from alumina vessel, in which the pyrolyzed material was placed, is considerable at this temperature. Since there is no aluminum in the SiOC matrix, it had to be built up into the structure of the wires by mixing with SiO and CO gases before deposition on the FeSi catalyst on the tip. No aluminum was found on the wires obtained at 1400 °C.

These 1D nanostructures are formed by a Vapor–Liquid-Solid (VLS) mechanism [30, 34–36]. Iron silicides that are on tips of the whiskers and wires are formed at high temperatures starting from 1200 °C. They arise as a result of an interaction of the SiOC matrix with decomposition products of the iron salt added to the ceramic precursor. Their catalytic interaction with SiO and CO gases, originating from the decomposition of the SiOC material, leads to the growth of nano-whiskers or nano- or micro-wires formed from these gaseous products. The growth does not occur equally from all spheroidal particles and from all their surfaces. Conditions favored for the growth are at the top layer of the particles where contact with reactive gases is most intensive. The external surfaces of the particles experience a more intensive action of the reactive gases than the surfaces of pores, thus the nano-whiskers seen at 1200 °C exude from the external surfaces. On the other hand, the conditions for nucleation of the wires are better at the walls of pores where concentrations of iron are higher. This is the reason for the formation of larger tips inside pores; consequently the wires seeded in the pores are thicker. Their nucleation is slow, but their growth is fast, which leads to unequal growth of the wires.

4 Conclusions

Preceramic macroporous microspheroidal polysiloxane particles containing $FeCl_3$ retain their shape and porosity on heating for a long times up to 1200 °C. Both dilatometry and mercury intrusion showed that their porosity is high, above 60%, and most pores are open. The particles heated at 600 °C display also a high mezoporosity. Ceramic macroporous microspheroidal SiOC particles and ceramer SiOC particles of hierarchical macro-mezo-microporosity are available by this simple procedure. The particles may be decorated with whiskers and wires if the temperature of the racemization is 1200–1400 °C. These 1D structures appear

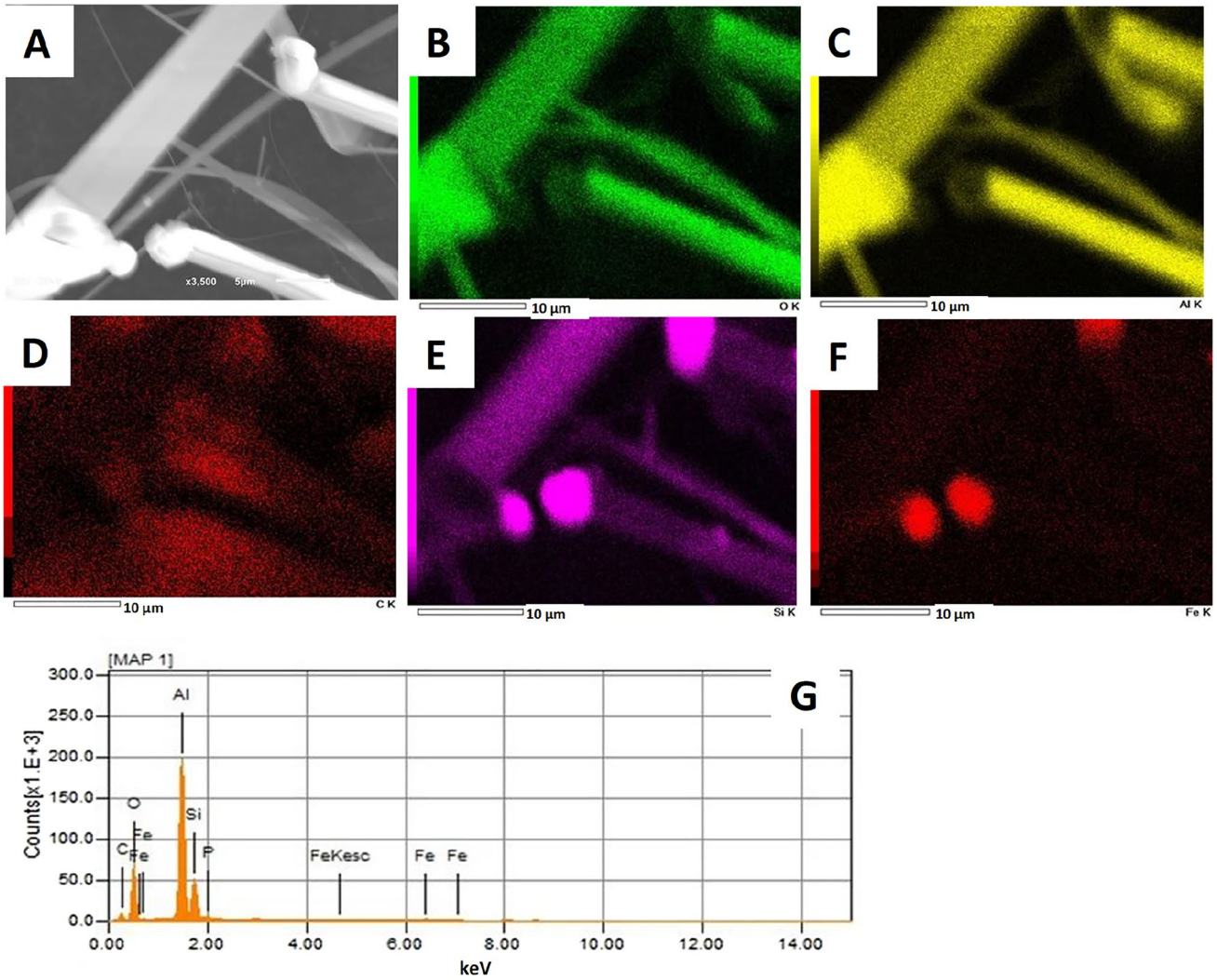

Fig. 10 **a**–**g** Mapping analysis of the cobweb of the area shown in SEM micrograph A. SEM micrographs represent maps of elements: **b** oxygen, **c** aluminum, **d** carbon, **e** silicon and **f** iron. Figure **g** shows the EDS spectrum

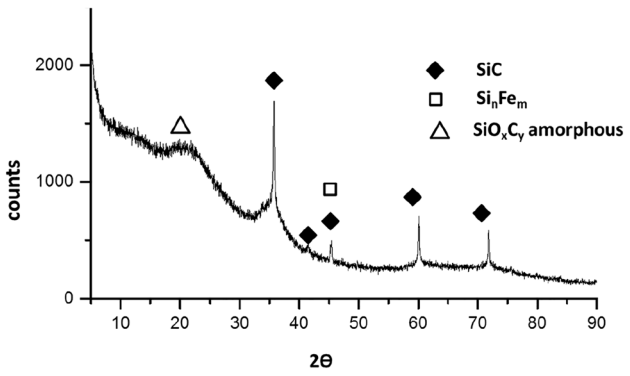

Fig. 11 X-ray diffractogram of the polysiloxane particles heated at 1400 °C

by a VLS mechanism. The whiskers outgrow from the external surfaces of particles pyrolyzed at 1200 °C. Wires are formed at still higher temperatures and most of them are seeded in pores.

Acknowledgements This research was supported by Center of Molecular and Macromolecular Studies, Polish Academy of Sciences. The authors are indebted to Dr. Martel Zeldin from the University of Richmond for valuable discussion and the improvement of the manuscript of this paper.

References

1. C. Stabler, E. Ionescu, M. Graczyk-Zajac, I. Gonzalo-Juan, R. Riedel, Silicon oxycarbide glasses and glass-ceramics, All-Rounder materials for advanced structural and functional applications. J. Am. Ceram. Soc. **101**, 4817–4856 (2018)
2. B. Xiao, X. Chen, R. Liang, Y. Zhang, Li, NiO microspheres with tunable porosity and morphology effects for CO oxidation. Catal. Sci. Technol. **1**, 999–1005 (2011)
3. Y. Liu, L. Wang, J. Zhang, F. Chen, M. Anpo, Preparation of Macroporous SAPO-34 microspheres by a spray drying method using polystyrene spheres as hard template. Res. Chem. Intermed. **37**, 949–959 (2011)
4. W. He, D. Min, X. Zhang, Y. Zhang, Z. Bi, Y. Yue, Hierarchically nanoporous bioactive glasses for high efficiency immobilization of enzymes. Adv. Funct Mater. **24**, 2206–2215 (2014)
5. J.S. Lee, J.K. Park, Processing of porous ceramic spheres by pseudo double emulsion method. Ceram. Int. **29**, 271–278 (2003)
6. A.R. Studart, U.T. Gonzenbach, E. Tervoort, L.J. Gauckler, Processing routes to macroporous ceramics. A review. J. Am. Ceram. Soc. **89**, 1771–1789 (2006)
7. T.Y. Klein, L. Treccani, K. Rezwan, Ceramic microbeads as adsorbents for purification technologies with high specific surface area, adjustable pore size, and morphology obtained by ionotropic gelation. J. Am. Ceram. Soc. **95**(3), 907–914 (2012)
8. J.J. Kirkland, F.A. Truszkowski, C.H. Dilks Jr., G.S. Engel, Superficially porous silica microspheres for fast high performance liquid chromatography of macromolecules. J. Chromatogr. A **890**, 3–13 (2000)
9. C. Vakifahmetoglu, M. Buldu, A. Karakuscu, A. Ponzoni, D. Assefa, G.D. Soraru, High surface area carbonous components from emulsion derived SiOC and their gas sensing behavior. J. Eur. Ceram. Soc. **35**, 4447–4452 (2015)
10. Y. Du, H. Liu, J. Shuang, J. Wang, J. Ma, S. Zhang, Microsphere-based selective laser sintering for building macroporous bone scaffolds with controlled microstructure and excellent biocompatibility. Colloids Surf. B **135**, 81–89 (2015)
11. D.L. Elbert, Liquid-liquid two-phase systems for the production of porous hydrogels and hydrogel microspheres for biomedical application. A tutorial review. Acta Biomater. **7**, 31–56 (2011)
12. C. Vakifahmetoglu, M. Balliana, P. Colombo, Ceramic foams and microbeads from emulsions of a preceramic polymer. J. Eur. Ceram. Soc. **31**, 1481–1490 (2011)
13. C. Ye, A. Chen, P. Colombo, C. Martinez, Ceramic microparticles and capsules via microfluidic processing of a preceramic polymer. J. R. Soc. Interface **7**(suppl_4), S461–S473 (2010)
14. Y. Hwang, D.H. Riu, K.J. Kim, C.H. Chang, Porous SiOC beads by freeze-drying polycarbosilane emulsions. Mater. Lett. **131**, 174–177 (2014)
15. V. Naglieri, P. Colombo, Ceramic microspheres with controlled porosity by emulsion-ice templating. J. Eur. Ceram. Soc. **37**, 2559–2568 (2017)
16. M. Nangrejo, E. Bernardo, P. Colombo, U. Farook, Z. Ahmad, E. Stride, M. Edirisinghe, Electrodynamic forming of porous ceramic capsules from a preceramic polymer. Mater. Lett. **63**, 483–485 (2009)
17. P. Pospiech, J. Chojnowski, U. Mizerska, W. Fortuniak, S. Slomkowski, J. Stolarski, Macroporous microspheres and microspheroidal particles from polyhydromethylsiloxane. Colloid Polym. Sci. **295**, 939–944 (2017)
18. D. Ding, J. Wang, G. Xiao, Z. Li, B. Bai, J. Ren, G. He, Enhanced magnetic wave absorbing properties of Si-O-C ceramics with in situ formed 1D nanostructures. Int. Appl. Ceram. Technol. (2019). https://doi.org/10.1111/ijac.13338
19. B. Du, J. Qian, P. Hu, C. He, M. Cai, X. Wang, A. Shui, Enhanced electromagnetic wave absorption of Fe-doped silicon oxycarbide nanocomposites. J. Am. Ceram. Soc. **103**(3), 1732–1743 (2019)
20. W. Duan, X. Yin, C. Luo, J. Kong, F. Ye, H. Pan, Microwave-absorption properties of SiOC ceramics derived from novel hyperbranched ferrocene-containing polysiloxane. J. Eur. Ceram. Soc. **37**(5), 2021–2030 (2017)
21. M. Adam, C. Vakifahmetoglu, P. Colombo, M. Wilhelm, G. Grathwohl, Polysiloxane-derived ceramics containing nanowires with catalytically active tips. J. Am. Ceram. Soc. **97**(3), 959–966 (2014)
22. W. Fortuniak, J. Chojnowski, S. Slomkowski, A. Nyczyk-Malinowska, P. Pospiech, U. Mizerska, Solid ceramic SiCO microspheres and porous rigid siloxane microspheres from swellable polysiloxane particles. Mater. Chem. Phys. **155**, 83–91 (2015)
23. W. Fortuniak, P. Pospiech, U. Mizerska, J. Chojnowski, S. Slomkowski, A. Nyczyk-Malinowska, R. Lech, M. Hasik, SiCO ceramic microspheres produced by emulsion processing and pyrolysis of polysiloxanes of various structures. Ceram. Int. **42**, 11654–11665 (2016)
24. W. Fortuniak, P. Pospiech, U. Mizerska, J. Chojnowski, S. Slomkowski, A. Nyczyk-Malinowska, A. Wojteczko, E. Wisla-Walsh, M. Hasik, Generation of mezo and microporous structures by pyrolysis of polysiloxane microspheres and by HF etching of SiOC microspheres. Ceram. Int. **44**, 374–383 (2018)
25. W. Szymanski, S. Lipa, W. Fortuniak, J. Chojnowski, P. Pospiech, U. Mizerska, S. Slomkowski, A. Nyczyk-Malinowska, M. Hasik, Silicon oxycarbide (SiOC) ceramic microspheres—structure and mechanical properties by nanoindentation studies. Ceram. Int. **45**, 11946–11954 (2019)
26. J. Chojnowski, S. Slomkowski, W. Fortuniak, U. Mizerska, P. Pospiech, Hydrophilic polysiloxane microspheres and ceramic SiOC microspheres derived from them. J. Inorg. Organomet. Polym. Mater. **30**(1), 56–68 (2020)
27. T. Prenzel, M. Wilhelm, K. Rezwan, Pyrolyzed polysiloxane membranes with tailorable hydrophobicity, porosity and high specific surface area. Micropor. Mesopor. Mater. **169**, 160–167 (2013)
28. M. Adam, M. Wilhelm, G. Grathwol, Polysiloxane derived hybrid ceramics with nanodispersed Pt. Micropor. Mesopor. Mater. **151**, 195–200 (2012)
29. M. Hojamberdiev, R.M. Prasad, C. Fasel, R. Riedel, E. Ionescu, Single-source-precursor synthesis of soft magnetic Fe_3Si- and Fe_5Si_3- containing SiOC ceramic nanocomposites. J. Eur. Ceram. Soc. **33**, 2465–2472 (2013)
30. C. Vakifahmetoglu, E. Pippel, J. Waltersdorf, P. Colombo, Growth of one-dimensional structure in porous polymer-derived ceramics by catalyst-assisted pyrolysis. Part I: iron catalyst. J. Am. Ceram. Soc. **93**, 959–968 (2010)
31. N.V. Godoy, J.L. Pereira, E.H. Duarte, C.R.T. Tarley, M.G. Segatelli, Influence of activated charcoal on the structural and morphological characteristics of ceramic based on silicon oxycarbide (SiOC): a promising approach to obtain a new electrochemical sensing platform. Mater. Chem. Phys. **175**, 33–45 (2016)
32. A. Saha, R. Raj, Crystallization maps for SiCO amorphous ceramics. J. Am. Ceram. Soc. **90**, 578–583 (2007)
33. A.L. Ortiz, F. Sanchez-Bajo, F.L. Cumbrera, F. Guiberteau, X-ray powder diffraction analysis of a silicon carbide-based ceramic. Mater. Lett. **49**, 137–145 (2001)

34. R.S. Wagner, W.C. Ellis, Vapor-liquid-solid mechanism of single crystal growth. Appl. Phys. Lett. **4**, 89–90 (1964)
35. A. Berger, E. Pippel, J. Woltersdorf, M. Scheffler, P. Cromme, P. Greil, Nanoprocesses in polymer-derived SiOC Ceramics: electron microscopic observations and reaction kinetics. Phys. Status Solid. A **202**, 2277–2286 (2005)
36. V. Vijay, V.M. Biju, R. Devasia, Active filler controlled polymer pyrolysis—a promising route for the fabrication of advanced ceramics. Ceram. Int. **42**, 15592–15596 (2016)